Shift and width of the H_α line of hydrogen in dense plasmas

St. Böddeker
Institut für Experimentalphysik V, Ruhr-Universität, 4630 Bochum, Germany

S. Günter and A. Könies
Fachbereich Physik, Universität Rostock, 0-2500 Rostock, Germany

L. Hitzschke
Osram A.G., 8000 München, Germany

H.-J. Kunze
Institut für Experimentalphysik V, Ruhr-Universität, 4630 Bochum, Germany
(Received 16 November 1992)

The profile and the shift of the H_α line of hydrogen were measured and the shift was calculated at high electron densities in a helium plasma. The plasma was produced in a gas-liner pinch, which was diagnosed by Thomson scattering. Densities were between 1×10^{18} cm^{-3} and 1×10^{19} cm^{-3} and temperatures varied from 4 up to 12.5 eV. The results show a nonlinear behavior of the shift. Corresponding theoretical calculations have been performed, especially taking into account the dynamic screening of the electron-atom interaction. The agreement is very good for densities below 5×10^{18} cm^{-3}; above that density it is satisfactory.

PACS number(s): 52.25.Rv, 32.70.Jz

I. INTRODUCTION

The H_α line of hydrogen emitted by plasmas is one of the most extensively studied spectral lines in theory and in experiment. Its shape and its width reflect to a certain degree microscopic processes within the plasma, and the analysis of its shape and its width as a function of electron density and temperature offers thus an opportunity to study these processes and to check new theoretical approaches developed to describe the interactions between the particles in a plasma [1]. Recently, calculations were carried out which extended shift predictions to very dense plasmas [2]. One of the most interesting results was the prediction of a marked deviation from the linear dependence of the electron-shift contribution on the density above 2×10^{18} cm^{-3} [2], which occasioned both experimental investigations and extended theoretical calculations. A slight nonlinearity with density had already been invoked in Ref. [3].

Earlier experiments reached only densities of 1×10^{18} cm^{-3} [4,5] and indeed did not show any deviations from linearity. We now employed the gas-liner pinch for such investigations [6], where higher densities are possible. Electron densities and temperature are determined independently by collective Thomson scattering. Investigations of the radial density and temperature profiles verified the expected homogeneity. The optical thickness of the H_α line was checked, and only for electron densities below 2×10^{18} cm^{-3} was the line profile affected. The shift was not affected, all spectra were reasonably well approximated by symmetrical, nearly Lorentzian profiles.

Theoretical values for the shifts were calculated according to the approach given in detail in Ref. [2] for the plasma parameter measured in the present experiment. The agreement between experiment and theory is indeed fairly good. In addition the shift was calculated following the theory by Griem [3,7–9].

II. EXPERIMENT

The gas-liner pinch has been described previously (e.g., [6,10,11]). A detailed description of the present device may be found in [6], so that only the main features are mentioned here.

In principle, it is a large-aspect-ratio z pinch. A driver gas and a test gas are independently injected into the discharge tube by two fast acting electromagnetic valves. The driver gas flows along the wall and forms initially a hollow cylinder. The test gas, whose final concentration amounts to a few percent of the driver gas, is puffed into the tube along the axis through the center of the upper electrode.

After preionization, an 11.1-μF main capacitor bank is discharged and the initial plasma shell is accelerated toward the center where the final plasma column is formed. It has a diameter of about 1.5 cm and a length of 5 cm. By proper choice of injection times and initial gas pressures one is able to confine the test gas to a small volume on the axis. Thus all lines of interest are emitted by test gas atoms from a region where the plasma is rather homogeneous in density and temperature; all lines are observed side on through four ports. For the present investigations we used helium as driver gas at a high initial pressure and hydrogen as test gas. The discharge energy was 3.5 kJ.

Density and temperature measurements were done by collective Thomson scattering using a ruby laser as described earlier in [12]. The detector system consisted of a 1-m monochromator (SPEX No. 1704) with a 1200-line/mm plane grating blazed at 1 μm and an optical multichannel analyzer (OMA) at the exit slit. Initially, this was model IRY-700G with 700 sensitive channels from Spectroscopy Instruments; later it was EG&G model 1456B-990G with 990 active channels. The reciprocal dispersion of both detection systems was 0.063 Å/channel, and the apparatus profile was 4–5 channels.

For the observation of the H_α line we used the same detection system as for Thomson scattering, but now with lower resolution. Thus we installed a 600-line/mm plane grating blazed at 5000 Å. When using an entrance slit of 30 μm, we measured a resolution of 0.414 Å/channel with both OMA systems. The apparatus profile was then 3–4 channels wide. To eliminate radiation from second and higher orders, a GG385 filter was used. The OMA systems were gated for an exposure time of 30 ns. During this time the plasma could be considered as quasistationary. The plasma lifetime was about 1 μs, the implosion time 3.0 μs.

The spectral emission of a tungsten strip lamp was used to calibrate all channels, and their relative sensitivity was taken into account when analyzing each spectral profile. The reproducibility of the discharge was controlled by recording the plasma continuum radiation at 5200 Å by a $\frac{1}{4}$-m monochromator equipped with an RCA 1P28 photomultiplier. The experimental setup is shown in Fig. 1.

III. THEORY

The Green's-function approach, which will be applied here to calculate spectral line profiles, is given in detail in Refs. [2,13,14]. There, the influence of dynamic screening of the electron-atom interaction on the shift of the hydrogen H_α line has been discussed for electron densities up to 2×10^{18} cm^{-3}. For even higher electron densities, a nonlinear behavior of the line shift with respect to the electron density had been suggested.

The self-energy and the vertex contributions to shift and width of spectral lines were given within a first-order Born approximation. It was found that the vertex contribution to the shift is rather small. For this reason only the self-energy Σ will be considered here to investigate dynamic screening effects on the line shift. Within a first-order Born approximation with respect to the dynamically screened perturber-radiator interaction the self-energy is given by

$$\Sigma_{HF}(E_n)=\sum_\alpha \int \frac{d\mathbf{q}}{(2\pi)^3}\int \frac{d\omega}{\pi}V(q)[1+n_B(\omega)] \times \frac{\mathrm{Im}\epsilon^{-1}(\mathbf{q},\omega+i\delta)}{E_n^0(\beta)-E_\alpha^0(\beta)-\omega} \times |M_{n\alpha}^{(0)}(\mathbf{q})|^2 . \quad (1)$$

As shown in Ref. [2], many-particle effects are retained only in the inverse dielectric function $\epsilon^{-1}(\mathbf{q},\omega)$ for bound-state contributions according to atomic polarizability. In formula (1), $V(q)$ is the Coulomb potential $V(q)=4\pi e^2/q^2$ and $n_B(\omega)$ represents the Bose distribution function $n_B(\omega)=(e^{\beta\omega}-1)^{-1}$. The isolated vertex function $M_{n\alpha}^{(0)}(\mathbf{q})$ is described in detail in Ref. [2]. The energies $E_n^0(\beta)$, $E_\alpha^0(\beta)$ denote the energy values of the radiator including the linear Stark effect due to the ionic microfield $E_n^0(\beta)=E_n^0+C(\beta)$.

When calculating hydrogen spectral lines for low-density plasmas different approximations may be applied instead of the full expression

$$\mathrm{Im}\epsilon^{-1}(\mathbf{q},\omega)=-\frac{\mathrm{Im}\epsilon(\mathbf{q},\omega)}{[\mathrm{Re}\epsilon(\mathbf{q},\omega)]^2+[\mathrm{Im}\epsilon(\mathbf{q},\omega)]^2} . \quad (2)$$

It follows from Eq. (1) that the main contributions to the self-energy shift arise where $\omega\approx E_n^0-E_\alpha^0$. That means the inverse dielectric function has to be considered at field frequencies which are comparable to the unperturbed transition frequencies $E_n^0-E_\alpha^0$.

So, considering virtual transitions between states of different principal quantum numbers ($\Delta n\neq0$), the energy difference $\omega_{n\alpha}=E_n^0-E_\alpha^0$ turns out to be much larger than the electron plasma frequency $\omega_{pe}=(n_e e^2/\epsilon_0 m_e)^{1/2}$. Therefore a binary-collision approximation may be applied. Within this approximation, the imaginary part of the inverse dielectric function is given by

$$\mathrm{Im}\epsilon^{-1}(\mathbf{q},\omega)\approx-\mathrm{Im}\epsilon(\mathbf{q},\omega) \quad (3)$$

which leads to a linear behavior of the electronic contribution to the line shift with respect to the free-electron density.

On the other hand, for virtual transitions between states of the same principal quantum number ($\Delta n=0$), the energy difference of these levels may be neglected compared with the electron plasma frequency. As a consequence, a static Debye screening can be taken for the inverse dielectric function

$$\mathrm{Im}\epsilon^{-1}(\mathbf{q},\omega)\approx-\frac{\mathrm{Im}\epsilon(\mathbf{q},\omega)}{(1+\kappa_D^2/q^2)^2} , \quad (4)$$

where κ_D is the inverse Debye radius

$$\kappa_D^{-1}=\left[\sum_a \frac{e_a^2 n_a}{\epsilon_0 k_B T}\right]^{1/2}=r_D . \quad (5)$$

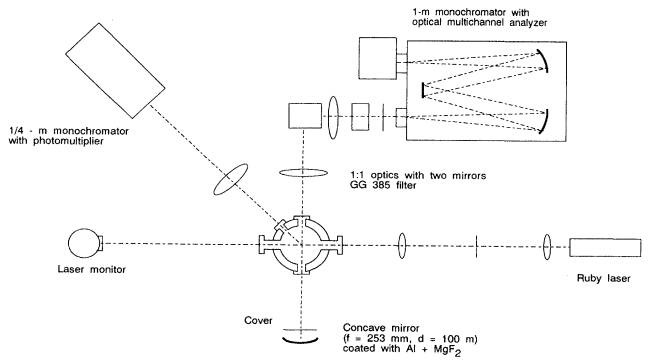

FIG. 1. Schematic of the experimental setup.

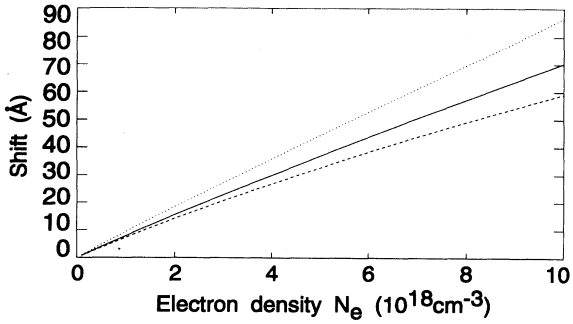

FIG. 2. Electron contribution to the shift of the upper level 322 due to virtual $\Delta n = 1$ transitions including dynamic screening (solid line) compared with the shift according to Griem [3] (dotted line) and the shift resulting from static Debye screening (dashed line).

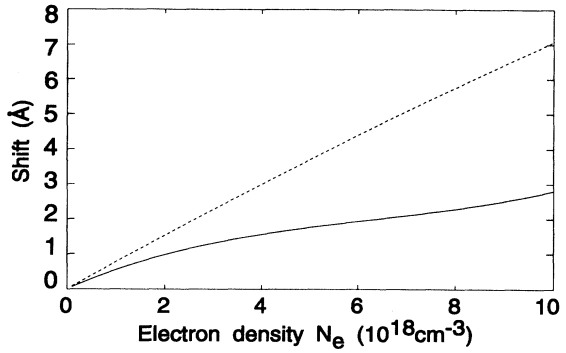

FIG. 3. Electronic contribution to the shift of the upper level 322 due to virtual $\Delta n = 0$ transitions including dynamic screening (solid line) compared with the shift resulting from static Debye screening (dashed line).

Static Debye screening for $(\Delta n = 0)$ transitions was used by Griem [3]. As the main contributions to the line shift result from $(\Delta n \neq 0)$ transitions, a nearly linear behavior of the electronic contribution to the line shift results for low-density plasmas.

For the dense plasmas considered here, however, approximations (3) and (4) have to be avoided because the ion-field-dependent energy distances between the perturbed and the neighboring perturbing energy levels become comparable to the electron plasma frequency. In this case, dynamic screening effects are important. Instead of the approximations (3) and (4), now the full expression for the imaginary part of the inverse dielectric function is to be evaluated. For the following calculations, the random phase approximation will be applied to describe the atomic polarization [14]. The latter is expanded to first order in V, and the corresponding weak collision contribution is multiplied with a factor of 1.2 to allow for close collisions [3].

In Figs. 2 and 3 the electronic contributions to the shift of the upper level (322) due to virtual $(\Delta n = 1)$ and $(\Delta n = 0)$ transitions, respectively, are shown. The shift including dynamic screening effects is compared with the shift calculated according to Griem [3] and the shift which results from Debye screening. As can be seen, for densities higher than 2×10^{18} cm^{-3}, noticeable deviations from a linear behavior occur. At a density of 10^{19} cm^{-3}, the deviations due to dynamic screening effects are remarkable, especially for the $(\Delta n = 0)$ transitions.

As mentioned above, for hydrogen lines it is necessary to consider not only the energy distance between the levels of different principal quantum numbers but also the splitting of the energy levels due to the linear Stark effect. At an electron density of about 8×10^{18} cm^{-3}, the splitting of the upper energy level becomes comparable to the electron plasma frequency. This leads to a slight swerve in the curve in Fig. 3.

In order to compare the H_α line shift with experimental results, we have to start with the full line profile

$$L(\Delta\omega) \propto \sum_{i,f} I_{if}(\Delta\omega) \int_0^\infty W_\rho(\beta)\, d\beta \times \mathrm{Im}\left\langle i \left| \left\langle f \left| \frac{1}{\omega - \omega_{if}^{(0)} - [\mathrm{Re}\Sigma_i(\beta) + \mathrm{Re}\Sigma_f(\beta)] + (i/2)[\mathrm{Im}\Sigma_i(\beta) + \mathrm{Im}\Sigma_f(\beta)] + i\Gamma^V} \right| f \right\rangle \right| i \right\rangle . \quad (6)$$

Here, $I_{if}(\Delta\omega)$ denotes the intensity of the transition $i \rightarrow f$ including the trivial asymmetry and $W_\rho(\beta)$ the ion microfield distribution function [15]. Σ and Γ^V are the self-energy and the vertex contribution, respectively [2], which describe the electron effects.

Besides the linear Stark effect resulting in a splitting of the energy levels, the quadratic Stark effect has to be taken into account. Furthermore, the ionic quadrupole shift due to the influence of the ionic field gradients on the radiator must be included [16]. Corrected wave functions have to be introduced in order to evaluate the intensities of the various Stark components $I_{if}(\omega_0)$, using a perturbation approach which includes the quadrupole shift and the quadratic Stark effect. For more details see, e.g., Ref. [16]. In this manner, the shift of the hydrogen H_α line profile maximum was calculated which for $(\Delta n \neq 0)$ electron contributions then corresponds to Eqs. (357) etc. of Ref. [7].

IV. RESULTS AND DISCUSSION

The profile of the H_α line of hydrogen was recorded at different times during our discharge. Thomson scattering at these times yielded electron density values from 0.5×10^{18} cm^{-3} to 10×10^{18} cm^{-3} and plasma temperatures between 4 and 12.5 eV. At such high plasma densities electron-ion collisions are fast and electron and ion temperatures are equal [17]. This is confirmed by the

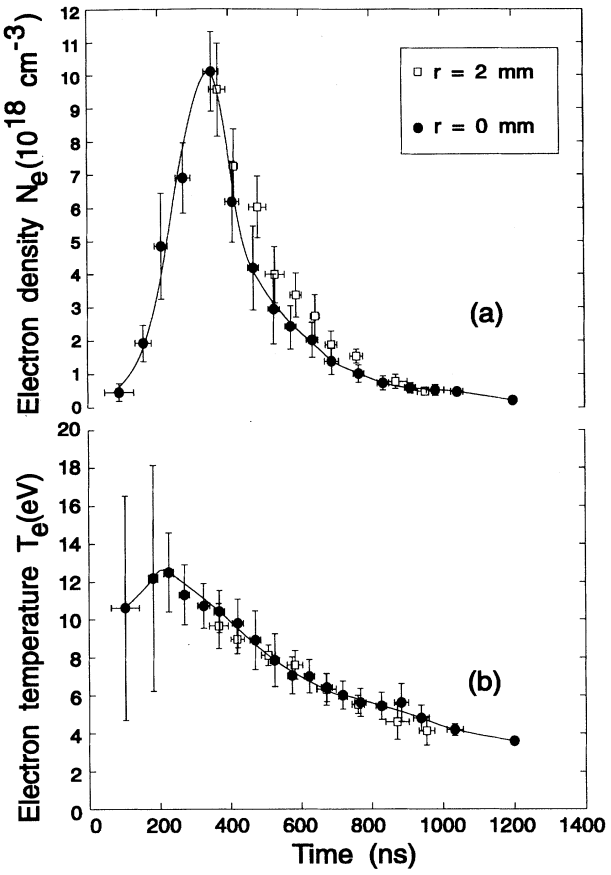

FIG. 4. Temporal evolution of (a) electron density and (b) plasma temperature on the axis ($r=0$) and at $r=2$ mm as obtained from Thomson scattering.

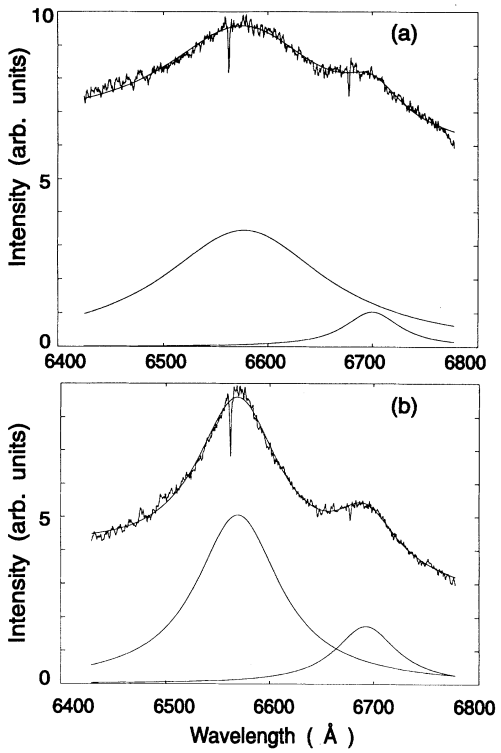

FIG. 5. Profiles of the H_α line and the He I line at 6678.15 Å recorded at two plasma densities: (a) $N_e=5.0\times10^{18}$ cm^{-3} and (b) $N_e=1.42\times10^{18}$ cm^{-3}. The Lorentzian functions shown are the best fit obtained.

shape of the spectral profile of the scattered radiation.

Figures 4(a) and 4(b) show the time evolution of electron density and temperature on the axis of the plasma column as well as at a position 2 mm off the axis. The diameter of the scattering volume was about 2 mm. The results confirm that the plasma is indeed homogeneous within the experimental error bars. These represent rms values from about 20 measurements at each position and time. They are about 15% for the density and 10% for the temperature after maximum compression and essentially reflect the reproducibility of the discharges. At early times, the variations from discharge to discharge are large on the axis, the plasma is highly dynamical, and spectroscopic observations were performed therefore only after maximum compression when the plasma has settled down and is in quasistationary equilibrium with the confining magnetic field.

Figures 5(a) and 5(b) each show a profile of the H_α line recorded at different times during the discharge. The pertinent electron densities from Thomson scattering are also given. The GG385 filter ensured that uv radiation, specifically the P_α line of He II at 3203 Å, was not present in second order. Discharges without hydrogen showed only the He I line at 6678.15 Å and a continuum intensity linearly varying with wavelength across the recorded wavelength interval. For this reason, each spectrum was fitted with two independent Lorentzian profiles, one for the H_α line and one for the He I line, and a linearly increasing continuum employing a least-squares fitting procedure [18]. The best-fit Lorentzian functions are shown in the figures for illustration. The strong continuum is also indicative of the high plasma density.

As can be seen, the fit of the H_α line by a Lorentzian shape was always very good, Stark broadening being the main broadening mechanism. The width of the apparatus profile was about 2 Å and broadening by Doppler effect amounted to 1.8 Å for the highest temperatures or about 1% of the full width at half maximum (FWHM) of the H_α line. At low densities, where also lower temperatures prevailed, the contribution of Doppler broadening to the linewidth was about 1.5%. For these reasons, apparatus profile and Doppler width could be neglected in all evaluations. The contribution of the He I line on the wing of the H_α line was important and had to be accounted for. It was responsible for the apparent asymmetry of the hydrogen line and increased its width. After it was subtracted, all profiles of the H_α line could be approximated by a Lorentzian.

Both lines showed self-absorption dips by atoms in the low-density region outside the compressed plasma column. At high densities, the width of the absorption dip of the H_α line reached 5 Å; it was fitted by a third Lorentzian profile which was included in the overall fitting procedure of both the H_α and the He I line. The

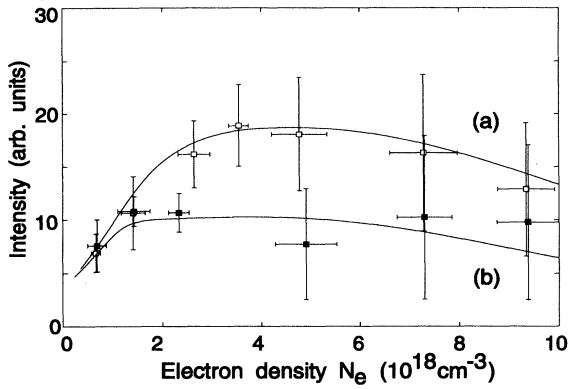

FIG. 6. Integrated intensities of the H_α line (a) with and (b) without a mirror behind the plasma column.

TABLE I. Experimental and theoretical values calculated by Kepple for the width (FWHM) of the H_α line for several electron densities and temperatures. The data in parentheses are calculated including only elastic-scattering contributions to the interference term as discussed in Refs. [20,21].

		Width (Å)	
N_e (10^{18} cm^{-3})	T_e (eV)	Expt.	Theor.
2.44	7.0	153±21	78(133)
3.44	7.6	182±24	104(171)
4.84	8.4	187±36	134(226)
7.08	9.2	228±64	180(322)
9.27	10.0	245±54	224(399)

absorption dips represented an excellent wavelength calibration and served as references for the evaluation of the line shifts.

The optical thickness of the H_α line was checked by placing a concave mirror ($f=253$ mm, coated with Al and MgF_2) behind the discharge column on the optical axis of the detection system. The center of curvature of the mirror was at the center of the plasma column, and thus one should obtain nearly doubling of the observed line intensities for optically thin lines. The whole system was calibrated by Rayleigh scattering (as usually done for Thomson scattering), first without and then with the mirror. The ratio of both intensities was 1.86.

Integrated H_α line intensities measured with and without the mirror are shown in Fig. 6 as a function of the electron density. The intensities above 2×10^{18} cm^{-3} are indeed doubled; below, however, optical thickness is evident. The intensities at the lower densities remained high since they were measured in the expansion and recombination phase of the plasma column. As the density decreases, the line becomes narrower and correspondingly the optical depth increases.

The spectra taken at electron densities below 2×10^{18} cm^{-3} were therefore not suitable to determine the full width of the line profile. For the higher densities, Table I gives the FWHM and the pertinent density and temperature. For the comparison with theory, one has to allow for the perturber charge. In the experiment presented here, the perturbers were singly and doubly ionized He atoms. The last column of Table I contains the FWHM calculated by Kepple according to Ref. [19] but including the full upper-level–lower-level interference (vertex) term in the electron broadening. The data in parentheses are calculated including only elastic-scattering contributions to the interference term as discussed in Refs. [20,21]. All values for the FWHM presented in Fig. 7 are depending on both electron temperature and density. The full triangles represent the theoretical values calculated by Kepple; the hollow triangles are the values in parentheses of Table I.

The optical depth observed at low densities does not affect the shift of the line profile, since all recorded profiles were symmetric. The shift was determined as the distance between the maximum of the fitted Lorentzian line profile and the unshifted line position. Table II gives this shift and the pertinent plasma parameters. The fourth column shows the theoretical shift calculated for these plasma parameters as discussed in Sec. III.

The last column presents the shifts calculated after Griem for the same parameters. These calculations were done following Refs. [7–9], extrapolating these values for the shifts at lower electron densities and temperatures to

TABLE II. Experimental and theoretical shift of the H_α line.

N_e (10^{18} cm^{-3})	T_e (eV)	$\Delta\lambda_{expt}$ (Å)	$\Delta\lambda_{theor,Günter}$ (Å)	$\Delta\lambda_{theor,Griem}$ (Å)
0.88	5.6	4.20±0.38	4.69	6.07
1.00	5.7	5.33±0.30	5.35	6.79
1.30	6.0	6.73±0.72	7.00	8.50
1.39	6.1	7.25±0.51	7.49	8.99
1.90	6.4	9.41±1.20	10.27	11.82
2.34	7.0	11.24±1.76	12.59	13.9
3.05	7.8	15.49±3.22	16.16	17.11
4.00	8.5	19.66±4.91	20.63	20.96
5.47	9.2	20.11±5.58	26.99	26.84
6.88	9.8	22.99±5.46	32.74	31.89
8.33	10.2	27.16±6.88	38.76	36.78
9.76	10.4	35.43±8.81	44.62	41.48

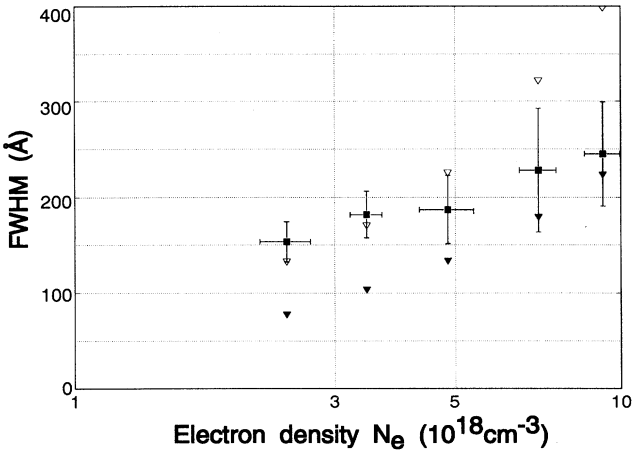

FIG. 7. Experimental (filled squares) and theoretical (filled triangles) data of the full width at half maximum of the H_α line vs the electron density. The hollow triangles represent the values in parentheses of Table I (see text). One has to note the different electron temperatures and ionic charges.

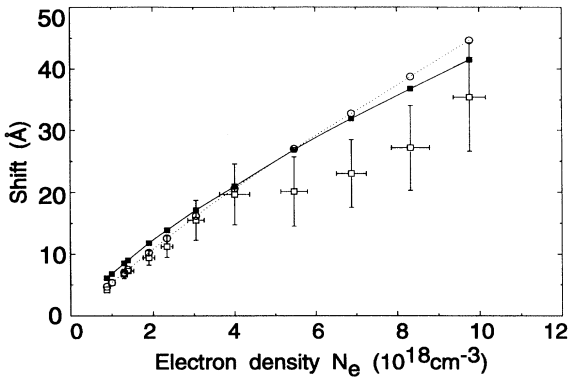

FIG. 8. Measured and calculated shift of the H_α line vs the electron density. The hollow circles represent the values from the presented calculations, the filled squares are the values calculated according to Griem. All values are calculated for the given experimental electron densities and temperatures.

our conditions. The different electron density, ionic charge, and temperature dependences of the various contributions to the total shift were taken into account. Different from our theory, the line shift is given by the sum of the ionic and the electronic contributions to the shift. Furthermore, for the central H_α component the shift resulting from ion collisions within the impact approximation according to Ref. [3] has been applied, instead of the quadratic Stark effect due to the static ionic microfield. This leads to smaller shifts compared to the shift calculated with static quadratic Stark effect. The errors for the ionic contributions are estimated to be a factor of 2 in both theoretical approaches, corresponding to $< 30\%$ error in the total shift.

In order to illustrate the observations, the experimental shift is plotted versus the electron density in Fig. 8. The error bars correspond to the rms values from about 20 discharges. The dotted line presents our theoretical results, the solid line the theoretical values calculated after Griem.

V. CONCLUSIONS

The H_α line of hydrogen has been measured in a helium plasma for electron densities higher than 1×10^{18} cm^{-3}. Line shift and full width were determined and the results are compared with corresponding calculations which were carried out for the present plasma conditions. The agreement for the shifts is very good for densities below 5×10^{18} cm^{-3}; for higher densities it is satisfactory. The scaling of the shift given by Griem also agrees with our measurements within estimated theoretical and experimental errors. Our measured widths favor the original profile calculations [19] at lower electron densities and calculations with the full upper-level–lower-level interference term in the electron broadening at higher densities [20,21]. Since these profile calculations are based on the quasistatic approximation for the broadening by ion-atom collisions, future calculations including ion dynamics will result in larger width, especially at lower densities. Such calculations have been performed [22] for $N_e \leq 10^{17}$ cm^{-3} and suggest that ion-dynamical corrections and differences in the interference term are then about the same.

ACKNOWLEDGMENTS

This work was supported by the Sonderforschungsbereich 191. The authors are grateful to H. R. Griem for discussions and helpful comments and to P. Kepple for his calculations of the full width.

[1] J. Callaway and K. Unnikrishnan, Phys. Rev. A **44**, 3001 (1991).
[2] S. Günter, L. Hitzschke, and G. Röpke, Phys. Rev. A **44**, 6834 (1991).
[3] H. R. Griem, Phys. Rev. A **38**, 2943 (1988).
[4] K. H. Finken, R. Buchwald, G. Bertschinger, and H.-J. Kunze, Phys. Rev. A **21**, 200 (1980).
[5] Y. Vitel, J. Phys. B **20**, 2327 (1987).
[6] H.-J. Kunze, in *Spectral Line Shapes,* edited by R. J. Exton (Deepak, Hampton, 1987), Vol. 4.
[7] H. R. Griem, *Spectral Line Broadening by Plasmas* (Academic, New York, 1974).
[8] H. R. Griem, Phys. Rev. A **28**, 1596 (1983).
[9] H. R. Griem (private communication).
[10] K. H. Finken and U. Ackermann, J. Phys. D **15**, 615 (1982).
[11] K. H. Finken and U. Ackermann, J. Phys. D **16**, 773 (1983).
[12] A. Gawron, S. Maurmann, F. Böttcher, A. Meckler, and H.-J. Kunze, Phys. Rev. A **38**, 4737 (1988).

[13] G. Röpke and L. Hitzschke, in *Spectral Line Shapes,* edited by J. Szudy (Ossolineum, Wroclaw, 1989), Vol. 5.
[14] L. Hitzschke, G. Röpke, T. Seifert, and R. Zimmermann, J. Phys. B **19**, 2443 (1986).
[15] C. F. Hooper, Phys. Rev. **165**, 215 (1968).
[16] J. Halenka, Z. Phys. D **16**, 1 (1990).
[17] L. Spitzer, Jr., Phys. Rev. **58**, 348 (1940).
[18] J. E. Dennis, Jr. and D. J. Woods, in *New Computing Environments: Microcomputers in Large-Scale Computing,* edited by A. Wouk (SIAM, Philadelphia, 1987), p. 116.
[19] P. Kepple and H. R. Griem, Phys. Rev. **173**, 317 (1968).
[20] D. Voslamber, Phys. Rev. A **14**, 1905 (1976).
[21] H. R. Griem and J. D. Hey, Phys. Rev. A **14**, 1906 (1976).
[22] R. L. Greene, J. Quant. Spectrosc. Radiat. Transfer **27**, 639 (1982).